

Review

# Constriction Channel Based Single-Cell Mechanical Property Characterization <sup>†</sup>

Chengcheng Xue <sup>1,\*</sup>, Junbo Wang <sup>1,\*</sup>, Yang Zhao <sup>1</sup>, Deyong Chen <sup>1</sup>, Wentao Yue <sup>2,\*</sup>  
and Jian Chen <sup>1,\*</sup>

Received: 2 September 2015 ; Accepted: 10 November 2015 ; Published: 16 November 2015

Academic Editors: Shih-Kang Fan, Da-Jeng Yao and Yi-Chung Tung

<sup>1</sup> State Key Laboratory of Transducer Technology, Institute of Electronics, Chinese Academy of Sciences, Beijing 100190, China; xuechengcheng13@mails.ucas.ac.cn (C.X.); zhaoyang110@mails.ucas.ac.cn (Y.Z.); dychen@mail.ie.ac.cn (D.C.)

<sup>2</sup> Department of Cellular and Molecular Biology, Beijing Chest Hospital, Capital Medical University, Beijing101149, China

\* Correspondence: jbwang@mail.ie.ac.cn (J.W.); yuewt@ccmu.edu.cn (W.Y.); chenjian@mail.ie.ac.cn (J.C.); Tel./Fax: +86-10-5888-7191 (J.W.); +86-10-8950-9373 (W.Y.); +86-10-5888-7531 (ext. 816) (J.C.)

<sup>†</sup> This paper is an extended version of our paper published in the 5th International Conference on Optofluidics 2015, Taipei, Taiwan, 26–29 July 2015.

**Abstract:** This mini-review presents recent progresses in the development of microfluidic constriction channels enabling high-throughput mechanical property characterization of single cells. We first summarized the applications of the constriction channel design in quantifying mechanical properties of various types of cells including red blood cells, white blood cells, and tumor cells. Then we highlighted the efforts in modeling the cellular entry process into the constriction channel, enabling the translation of raw mechanical data (e.g., cellular entry time into the constriction channel) into intrinsic cellular mechanical properties such as cortical tension or Young's modulus. In the end, current limitations and future research opportunities of the microfluidic constriction channels were discussed.

**Keywords:** single-cell analysis; microfluidics; constriction channel; mechanical property characterization; high throughput

---

## 1. Introduction

The mechanical properties of a biological cell are largely determined by the characteristics of its cytoskeleton, an elaborate network of fibrous proteins [1,2]. Various diseases and changes in cell states are reported to lead to variations in cellular mechanical properties, which include (1) changes in the stiffness of blood cells (e.g., variations of red blood cells (RBCs) in malaria or sickle cell anemia and white blood cells (WBCs) in sepsis, trauma, and acute respiratory distress syndrome); (2) increased cell deformability of invasive cancer cells; and (3) decreased deformability during the stem cell differentiation process [3,4].

Conventionally, cellular mechanical properties are quantified based on well-established techniques (e.g., atomic force microscopy, micropipette aspiration and optical tweezers) [3]. In atomic force microscopy, a probe tip attached to a flexible cantilever is pressed into the cell surface for a set distance with cantilever deflections measured and translated to cellular mechanical properties [5,6]. Although powerful, this approach is capable of quantifying cellular mechanical properties, which are dependent on experimental conditions (e.g., poking depth, rate, and position) [7]. To deal with this issue, multiple scans on the same cell are requested to collect trustworthy data, leading to a

compromised measurement speed with limited throughput (e.g., less than 10 cells per sample from patient pleural fluids based on atomic force microscopy [8]).

For micropipette aspiration, the surface of a cell is aspirated into a small glass tube with the leading edge of its surface tracked, which is further translated to cellular mechanical properties [9]. Compared with atomic force microscopy, micropipette aspiration deforms a cell patch in a more global manner, leading to more accurate characterization of cellular mechanical properties. However, this technique requires skilled operation on the glass pipette and thus proceeds with limited throughput (~10 cells per cell type from patient voided urine [10,11]).

Microfluidics is the manipulation and processing of fluids on micrometer scales ranging from one to hundreds of  $\mu\text{ms}$  [12,13]. Due to its dimensional match with biological cells, it has been used for single-cell analysis [14,15]. Currently, several microfluidic devices have been proposed to quantify the mechanical properties of single cells based on various mechanisms such as optical stretching, fluid stretching and constriction channels [16,17].

In a microfluidic optical stretcher, a two-beam laser is used to serially deform single suspended cells flowing within microfluidic channels for cellular mechanical property characterization [18,19]. In a microfluidic hydrodynamic stretcher, single cells are delivered to a micro channel with geometry variations, producing extensional fluid flow to cause cell deformation [20–22]. Although these two approaches are featured with significantly higher throughputs than conventional approaches, they can only collect cellular mechanical parameters (e.g., deformation ratio and elongation index), which remain dependent on cell sizes and experimental conditions (e.g., pressure drop, channel geometry) [17].

**Table 1.** Key developments in the field of microfluidic constriction channels enabling high-throughput cellular mechanical property characterization.

Cell Types	Quantified Parameters	Key Observations	References
Plasmodium falciparum infected RBCs	Channel blockage	Maturation of Plasmodium falciparum decreased the deformability of infected RBCs.	[23]
Plasmodium vivax infected RBCs	Channel blockage	No significant decrease in deformability was observed during the maturation of Plasmodium vivax infected RBCs.	[27]
Plasmodium falciparum infected RBCs	Transit velocity	The parasite protein Pf155 decreased the transit velocity of ring-stage infected RBCs.	[29]
Plasmodium falciparum infected RBCs	Cortical tension	Cortical tensions were quantified as $3.22 \pm 0.64 \text{ pN}/\mu\text{m}$ (uninfected RBCs), $4.66 \pm 1.15 \text{ pN}/\mu\text{m}$ (ring-stage infected RBCs), $8.26 \pm 2.84 \text{ pN}/\mu\text{m}$ (early trophozoite infected RBCs), and $21.38 \pm 5.81 \text{ pN}/\mu\text{m}$ (late trophozoite infected RBCs).	[30]
Plasmodium falciparum infected RBCs	Transit velocity	Artesunate (a drug in malaria) decreased the deformability of infected RBCs while it had no effect on normal RBCs.	[31]
Normal and oxidized RBCs	Cortical tension	Cortical tensions were quantified as $20.13 \pm 1.47 \text{ pN}/\mu\text{m}$ (normal RBCs) and $27.51 \pm 3.64 \text{ pN}/\mu\text{m}$ (oxidized RBCs).	[32]
White blood cells	Transit time	In diseases of sepsis and leukostasis, decreases in the deformability of WBCs were found.	[24]
Breast tumor cells	Entry time and transit velocity	Benign breast epithelial cells of MCF-10A had longer entry times than tumor breast cells of MCF-7 with similar sizes.	[25]
Lung tumor cells	Instantaneous Young's modulus	Instantaneous Young's moduli were quantified as $3.48 \pm 0.86 \text{ kPa}$ for A549 cells and $2.99 \pm 0.38 \text{ kPa}$ for 95C cells	[47]

Meanwhile, the microfluidic constriction channel is used to quantify the cellular entry and transition process through a micro channel with a cross-sectional area smaller than the dimensions

of a single cell, enabling high-throughput single-cell mechanical property characterization [23–26] (see Table 1). This technique was first used to evaluate the mechanical properties of RBCs [23,27–40], which was then expanded to study the deformability of WBCs [24,41,42] and tumor cells [25,43–45]. Leveraging mechanical modeling of the cellular entry process into the constriction channel, the microfluidic constriction channel design can collect size-independent intrinsic biomechanical markers such as cortical tension or Young’s modulus [35,46–48].

## 2. Constriction Channel Based Mechanical Property Characterization of Red Blood Cells

Initially, the constriction channel design was used to quantify the mechanical properties of RBCs [23,27–40]. In 2003, Chiu *et al.*, characterized complex behaviors of *Plasmodium falciparum* infected RBCs using the constriction channels with sizes at 8, 6, 4, and 2 μm in width [23] (see Figure 1a). Ring-stage infected RBCs resembled normal RBCs in morphology and were capable of passing through all constricted channels. Early and late trophozoite infected RBCs were noticed squeezing through the larger 8- and 6-μm channels but would block the smaller 4- and 2-μm channels. Schizont stage infected RBCs blocked all but the 8-μm channels (see Figure 1b). In addition, the same constriction channel design with 2-μm channels was used to probe the mechanical properties of *Plasmodium vivax* infected RBCs, revealing that in contrast to *Plasmodium falciparum*, *Plasmodium vivax* infected RBCs of all developmental stages were observed to transverse the 2-μm constriction readily [27].

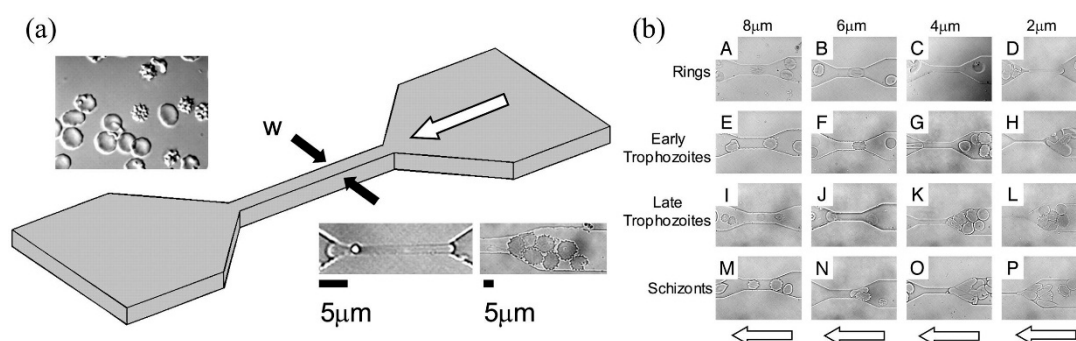


**Figure 1.** (a) Schematic illustration of the geometry of the constriction channel design which was sized at 8, 6, 4, and 2 μm in width. (Upper Inset) An image of normal (smooth) and infected RBCs. (Lower Inset) A normal RBC was passing through a 2-μm constriction and infected RBCs blocked a 6-μm constriction channel. (b) Four stages of malaria-infected RBCs through the constriction channels. Ring-stage infected erythrocytes were able to pass through all constriction channels. Early trophozoite and late trophozoite infected cells passed through the larger 8- and 6-μm channels but eventually blocked the smaller 4- and 2-μm channels. Schizont stage infected erythrocytes blocked all but the 8-μm channels. The arrows indicate direction of flow. Reproduced with permission from [23].

Using microfluidic constriction channels in parallel, the effect of Artesunate (a drug widely used for the treatment of malaria) on the dynamic deformability of RBCs infected with ring-stage *Plasmodium falciparum* malaria was also evaluated [31]. As shown in Figure 2a, a microfluidic device with triangular pillar arrays as repeated constrictions (inter-pillar gap sizes of 3 or 4 μm) was used and RBCs were deformed to pass through constriction channels in series (see Figure 2b). After the treatment of Artesunate, a 50% decrease in the transit velocity of *Plasmodium falciparum* infected RBCs was reported whereas only small (~10%) velocity reduction was observed among uninfected RBCs. These results demonstrated that ART alters the deformability of *Plasmodium falciparum* infected RBCs, which may influence blood circulation through micro vasculatures (see Figure 2c).

Furthermore, Ma *et al.*, accurately controlled the pressure applied across the constriction channels to obtain the critical pressure threshold requested to push each RBCs through the constriction positions. Based on an equivalent mechanical model, the threshold value was translated

to an intrinsic mechanical parameter, cortical tension (see Figure 3a) [30]. This approach was used to study the mechanical properties of *Plasmodium falciparum* infected RBCs, producing cortical tensions of  $3.22 \pm 0.64$  pN/ $\mu\text{m}$  for uninfected RBCs,  $4.66 \pm 1.15$  pN/ $\mu\text{m}$  for ring-stage infected RBCs,  $8.26 \pm 2.84$  pN/ $\mu\text{m}$  for early trophozoite infected RBCs, and  $21.38 \pm 5.81$  pN/ $\mu\text{m}$  for late trophozoite infected RBCs. In addition, the measured cortical tensions of schizont stage infected RBCs ranged from 85 to 1300 pN/ $\mu\text{m}$ , with an average value of 606 pN/ $\mu\text{m}$  (see Figure 3b).

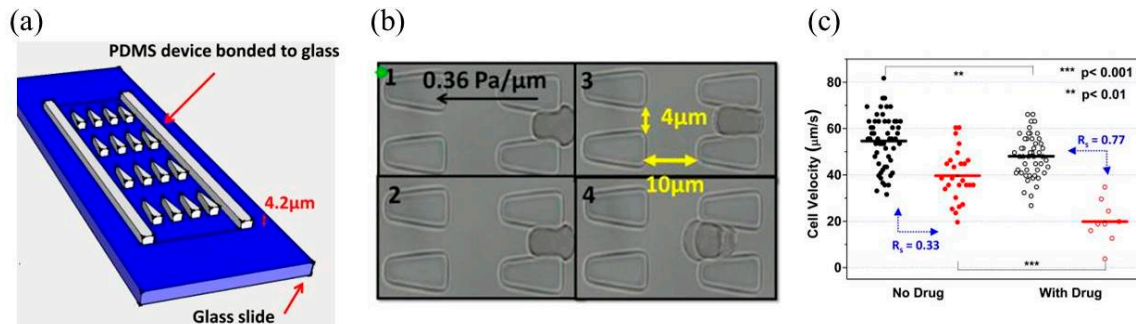


**Figure 2.** (a) Schematic of the geometry of the parallel constriction channel design; and (b) experimental images of RBCs passing through constriction positions; (c) The treatment of Artesunate significantly decreases the cell velocity of *Plasmodium falciparum* infected RBCs while it has no significant effect on uninfected RBCs. Reproduced with permission from [31].

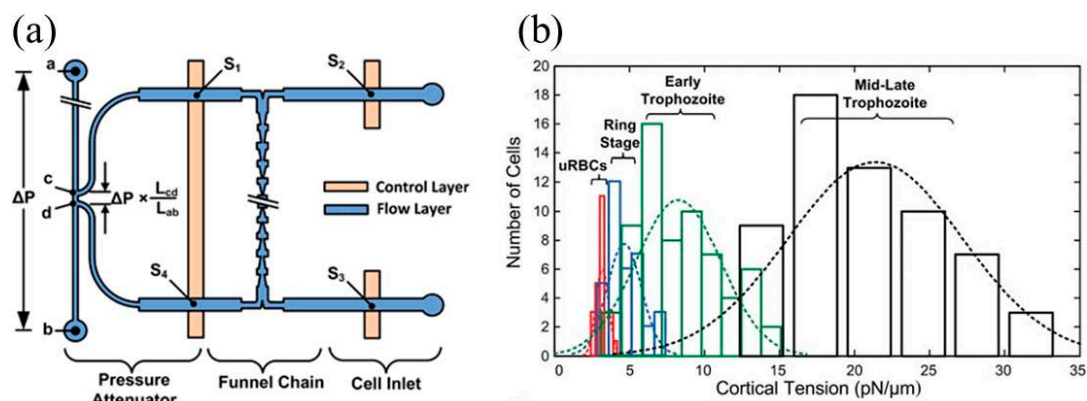


**Figure 3.** (a) Design of the flow and control layers of the microfluidic constriction channel capable of generating precisely controlled pressure to quantify the critical threshold requested to push each RBC through the constriction channel. In this study, the pressure regulator divides an externally applied pressure by a factor of 100, which is further applied across the funnel chain; (b) Histogram of the quantified cortical tensions of RBCs in various stages. Reproduced with permission from [30].

### 3. Constriction Channel Based Mechanical Property Characterization of White Blood Cells

The constriction channel design was also used to characterize the mechanical properties of WBCs [24,41,42,49]. Fletcher *et al.*, were pioneers in this field and proposed a network of constriction channels (~6  $\mu\text{m}$  wide) to characterize transit time of WBCs in diseases of sepsis and leukostasis (see Figure 4a) [24]. Experimental results show that (1) inflammatory mediators involved in sepsis significantly increased the transit time of WBCs (see Figure 4b); (2) altered mechanical properties of WBCs were found to correlate with symptoms of leukostasis in patients.

Furthermore, Theodoly *et al.*, explored the functions of actin organization and myosin II leveraging the constriction channel design, revealing that (1) cell stiffness depends strongly on the organization of F-actin rather than myosin II; (2) the actin network is not completely destroyed after

a forced travelling through the constriction channel; (3) myosin II plays a major role in maintaining cellular shapes [41].

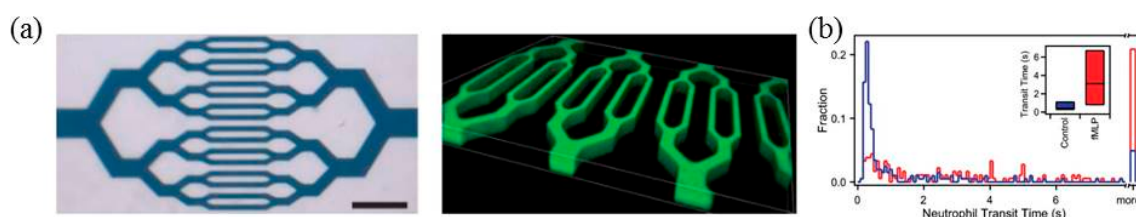


**Figure 4.** (a) Schematic of the constriction channel network for the mechanical property characterization of WBCs where the device trifurcates into a network of bifurcating channels including 64 parallel constriction channels; (b) The transit time of the neutrophil populations with or without fMLP exposure. Note that fMLP is an inflammatory mediator involved in sepsis. Reproduced with permission from [24].

#### 4. Constriction Channel Based Mechanical Property Characterization of Tumor Cells

The constriction channel design was further used to characterize and classify tumor cells based on their mechanical properties [25,43–45,50]. In 2008, Lim *et al.*, classified benign breast epithelial cells (MCF-10A) and non-metastatic tumor breast cells (MCF-7) using the constriction channel design, finding that MCF-10A had longer entry time than MCF-7 with similar sizes [25]. In addition, Vanapalli *et al.*, classified benign and cancerous brain cells using the constriction channels, revealing that compared to the cellular transit velocity within the constriction channels, cellular entry time into the constriction channel can provide more insights in differentiating these cell types [43]. Furthermore, Erickson *et al.*, proposed a microfluidic device with serial constriction channels to study the repeated deformability of tumor cells with and without the treatment of taxol. Experimental results show that (1) cells treated with taxol required longer transit times when travelling through the first constriction than untreated cells; (2) the initial transit required the longest time and subsequent transits were faster and the difference between the two cell groups was reduced (see Figure 5) [44].

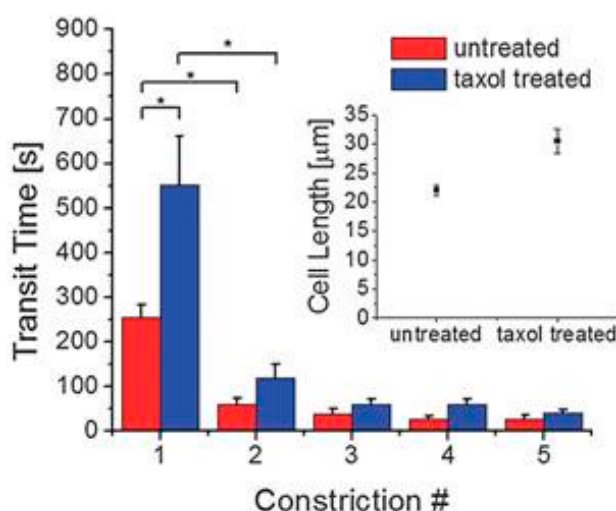


**Figure 5.** Cell permeation across sequential microfluidic constriction channels with the effects of taxol investigated. Cells treated with taxol were larger (inset) and required a longer transit time to cross the first constriction than untreated cells. For both cell groups, the initial transit required the longest time while subsequent transits were faster where the duration difference between the two cell groups was reduced. Reproduced with permission from [44].

### 5. Mechanical Modeling of the Constriction Channel Design

In the majority of the aforementioned studies, raw mechanical parameters including entry time, transit velocity and elongation index were commonly derived from the constriction channel design for cell type classification. However, these parameters are strongly dependent on cell sizes and experimental conditions (e.g., dimensions of the constriction channels and pressure applied to push cells through the constriction channels). Thus, they cannot reflect intrinsic cellular mechanical properties of single cells.

To address this issue, a few studies have been conducted to model the cellular entry process into the constriction channel which can translate these raw parameters into intrinsic cellular mechanical parameters such as Young’s Modulus and Cortical Tension [35,36,45–47,51,52]. Ma *et al.*, are pioneers in this field and they used a Newtonian liquid drop to model a RBC where the cell deformability is indicated by a persistent cortical tension of the cell membrane (see Figure 6) [35,46]. When each cell is constrained in a constriction channel, the cellular deformation can be divided into three sections: a leading portion, an internal section contacting the constriction, and a trailing portion (see Figure 6a). Based on this equivalent mechanical model, the quantified critical threshold pressure which can push an RBC through the constriction channel was transferred to cortical tensions. Based on this approach, the cortical tensions of neutrophils, lymphocytes, RT4 bladder cancer cells, and lymphoma cells were quantified as  $37.0 \pm 4.8$ ,  $74.7 \pm 9.8$ ,  $185.4 \pm 25.3$ , and  $235.4 \pm 31.0$  pN/ $\mu\text{m}$ , respectively (see Figure 6b).

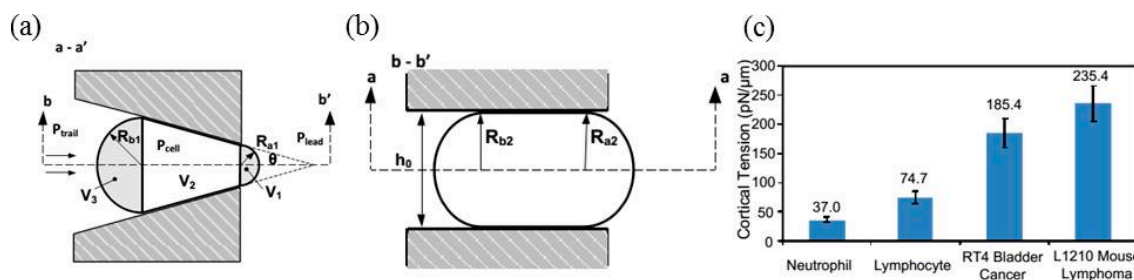


**Figure 6.** (a) Top view; and (b) side view illustration of a single RBC at the critical point of the constriction constriction; (c) Comparison of the quantified cortical tensions from four different cell types. Reproduced with permission from [46].

In addition, Theodoly *et al.*, modelled the cellular entry process into the constriction channel with the effects of friction and leakage taken into consideration [51]. As a follow-up study, Chen *et al.*, used a visco-hyperelastic solid to model a tumor cell using ABAQUS based numerical simulations where cell-channel wall frictions were modeled using a simple Coulomb law (see Figure 7) [47]. Both experiments and simulations confirmed the two-stage cellular entry process into the constriction channel: an instantaneous jump into the channel indicated by instantaneous aspiration length followed by a creeping increase in aspiration length which is terminated by transitional aspiration length (see Figure 7a). Numerical simulations reveal that instantaneous aspiration length and transitional aspiration length are reversely proportional to Young’s instantaneous modulus ( $E_{instantaneous}$ ), which are affected by friction coefficient regardless of other cellular viscoelastic parameters. By combining measured instantaneous aspiration length and transitional aspiration length with these obtained from numerical simulations,  $E_{instantaneous}$  of these two cells types were quantified as  $3.48 \pm 0.86$  kPa (A549 cells,  $n = 199$ ) and  $2.99 \pm 0.38$  kPa (95C cells,  $n = 164$ ) (see Figure 7b).

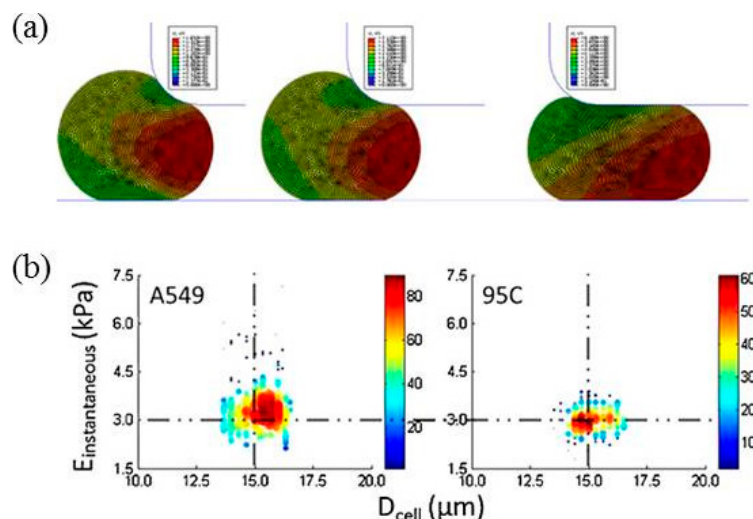


**Figure 7.** (a) Numerical simulations of the cellular entry process including initial jump into the channel (left), cellular creep response (middle) and creep response termination (right) at the transitional position. (b) Scatter plots of  $E_{\text{instantaneous}}$  (Instantaneous Young’s Modulus) vs.  $D_{\text{cell}}$  for A549 cells and 95C cells (two lung cancer cell lines), indicating noticeable differences in  $E_{\text{instantaneous}}$  between these two cell types. Reproduced with permission from [47].

## 6. Discussions

Due to dimensional comparison, the microfluidic constriction channel is a powerful tool in the field of single-cell analysis, which was used for quantifying cellular mechanical properties where single cells were flushed into the constriction channel with their entry times and transition velocities adopted as biophysical markers [23–25]. Furthermore, this tool was used for quantifying cellular electrical properties since the deformed cells effectively seal constriction channel walls, and block electric lines, enabling single-cell electrical property characterization [53–56]. Meanwhile, the constriction channel design was also used as a tool to study chemical synthesis of red blood cells [57] or deliver vector-free gene vectors [42,58].

In the field of constriction channel based single-cell mechanical property characterization, after roughly 10 years of intensive studies, two challenges have been carefully addressed. The first key progress is the capability of translating raw parameters such as entry time into intrinsic mechanical markers such as instantaneous Young’s modulus or cortical tension [35,46,47]. These raw mechanical parameters depend on cell sizes and experimental conditions. Thus, data reported by different groups cannot be effectively compared. Meanwhile, intrinsic mechanical parameters such as Young’s modulus and cortical tension are not affected by these environmental changes, and thus data collected from multiple centers can be collected and compared, which may help form detection thresholds in classifying corresponding diseases. Note that the up-to-date understanding of cells’ mechanical properties considers cells as a viscoelastic material and a comprehensive determination of a cell’s mechanical properties requires additional data such as relaxation time besides Young’s modulus or cortical tensions.

The second key progress is the proposal of constriction channels with adjustable cross-section areas to deal with the issue of channel blockage [59,60]. Since the dimensions of the constriction channel are smaller than single cells, there is a persistent concern of channel clogging due to unwanted microparticles. In recent studies, one fixed wall of the constriction channel was replaced with a thin membrane and its deflection was regulated by external pressure sources. If the constriction channel was blocked by solid particles or cell clusters, the application of pressure causes the deflection of the constriction channel walls, enlarging the cross-sectional area to remove the blocked particles.

This improvement in the constriction channel design can significantly improve the robustness of the device in the process of characterizing cellular mechanical properties [59,60].

Currently, the major limitation of the constriction channel based single-cell mechanical property characterization is the throughput, which is roughly one cell per second. Although this value is much higher than conventional techniques such as atomic force microscopy and micropipette aspiration (one cell per min), it is significantly lower than the throughput of flow cytometry at roughly 1000 cells per second and thus cannot collect data from thousands of single cells.

The second concern is whether mechanical markers alone are enough to classify cell types. For diseases with blood cells or tumors, there are heterogeneous cell types and it is highly doubtful that biomechanical markers alone can provide a sound evaluation. Currently, the constriction channel design was integrated with impedance spectroscopy to enable both electrical and mechanical property characterization of single cells [61–63]. Further studies may consider integrating the constriction channel design with other functional components to further enable the measurement of multiple parameters of single cells, providing a comprehensive evaluation of biological cells.

**Acknowledgments:** We thank the National Basic Research Program of China (973 Program, Grant No. 2014CB744600), the National Natural Science Foundation of China (Grant No. 61201077, 61431019 and 81261120561), and the Beijing NOVA Program of Science and Technology for financial support.

**Author Contributions:** C.X. reviewed the section of mechanical property characterization of red blood cells. J.W. reviewed the section of mechanical property characterization of white blood cells. Y.Z. reviewed the section of mechanical property characterization of tumor cells. D.C. reviewed the section of mechanical modeling of the constriction channel. W.Y. contributed to the section of discussion. C.X. and J.C. drafted the manuscript.

**Conflicts of Interest:** The authors declare no conflict of interest.

## References

1. Ethier, C.R.; Simmons, C.A. *Introductory Biomechanics: From Cells to Organisms*; Cambridge University Press: Cambridge, UK, 2007.
2. Fletcher, D.A.; Mullins, R.D. Cell mechanics and the cytoskeleton. *Nature* **2010**, *463*, 485–492. [[CrossRef](#)] [[PubMed](#)]
3. Di Carlo, D. A mechanical biomarker of cell state in medicine. *J. Lab. Autom.* **2012**, *17*, 32–42. [[CrossRef](#)] [[PubMed](#)]
4. Lee, G.Y.H.; Lim, C.T. Biomechanics approaches to studying human diseases. *Trends Biotechnol.* **2007**, *25*, 111–118. [[CrossRef](#)] [[PubMed](#)]
5. Alonso, J.L.; Goldmann, W.H. Feeling the forces: Atomic force microscopy in cell biology. *Life Sci.* **2003**, *72*, 2553–2560. [[CrossRef](#)]
6. Kirmizis, D.; Logothetidis, S. Atomic force microscopy probing in the measurement of cell mechanics. *Int. J. Nanomed.* **2010**, *5*, 137–145. [[CrossRef](#)]
7. Lekka, M.; Pogoda, K.; Gostek, J.; Klymenko, O.; Prauzner-Bechcicki, S.; Wiltowska-Zuber, J.; Jaczewska, J.; Lekki, J.; Stachura, Z. Cancer cell recognition—mechanical phenotype. *Micron* **2012**, *43*, 1259–1266. [[CrossRef](#)] [[PubMed](#)]
8. Cross, S.E.; Jin, Y.S.; Rao, J.; Gimzewski, J.K. Nanomechanical analysis of cells from cancer patients. *Nat. Nanotechnol.* **2007**, *2*, 780–783. [[CrossRef](#)] [[PubMed](#)]
9. Hochmuth, R.M. Micropipette aspiration of living cells. *J. Biomech.* **2000**, *33*, 15–22. [[CrossRef](#)]
10. Shojaei-Baghini, E.; Zheng, Y.; Jewett, M.A.S.; Geddie, W.B.; Sun, Y. Mechanical characterization of benign and malignant urothelial cells from voided urine. *Appl. Phys. Lett.* **2013**, *102*, 123704. [[CrossRef](#)]
11. Shojaei-Baghini, E.; Zheng, Y.; Sun, Y. Automated micropipette aspiration of single cells. *Ann. Biomed. Eng.* **2013**, *41*, 1208–1216. [[CrossRef](#)] [[PubMed](#)]
12. Whitesides, G.M. The origins and the future of microfluidics. *Nature* **2006**, *442*, 368–373. [[CrossRef](#)] [[PubMed](#)]
13. Wootton, R.C.; Demello, A.J. Microfluidics: Exploiting elephants in the room. *Nature* **2010**, *464*, 839–840. [[CrossRef](#)] [[PubMed](#)]

14. Weaver, W.M.; Tseng, P.; Kunze, A.; Masaeli, M.; Chung, A.J.; Dudani, J.S.; Kittur, H.; Kulkarni, R.P.; Di Carlo, D. Advances in high-throughput single-cell microtechnologies. *Curr. Opin. Biotechnol.* **2014**, *25*, 114–123. [[CrossRef](#)] [[PubMed](#)]
15. Sims, C.E.; Allbritton, N.L. Analysis of single mammalian cells on-chip. *Lab Chip* **2007**, *7*, 423–440. [[CrossRef](#)] [[PubMed](#)]
16. Kim, D.H.; Wong, P.K.; Park, J.; Levchenko, A.; Sun, Y. Microengineered platforms for cell mechanobiology. *Annu. Rev. Biomed. Eng.* **2009**, *11*, 203–233. [[CrossRef](#)] [[PubMed](#)]
17. Zheng, Y.; Nguyen, J.; Wei, Y.; Sun, Y. Recent advances in microfluidic techniques for single-cell biophysical characterization. *Lab Chip* **2013**, *13*, 2464–2483. [[CrossRef](#)] [[PubMed](#)]
18. Lincoln, B.; Erickson, H.M.; Schinkinger, S.; Wottawah, F.; Mitchell, D.; Ulvick, S.; Bilby, C.; Guck, J. Deformability-based flow cytometry. *Cytom. Part A* **2004**, *59*, 203–209. [[CrossRef](#)] [[PubMed](#)]
19. Guck, J.; Schinkinger, S.; Lincoln, B.; Wottawah, F.; Ebert, S.; Romeyke, M.; Lenz, D.; Erickson, H.M.; Ananthakrishnan, R.; Mitchell, D.; *et al.* Optical deformability as an inherent cell marker for testing malignant transformation and metastatic competence. *Biophys. J.* **2005**, *88*, 3689–3698. [[CrossRef](#)] [[PubMed](#)]
20. Gossett, D.R.; Tse, H.T.; Lee, S.A.; Ying, Y.; Lindgren, A.G.; Yang, O.O.; Rao, J.; Clark, A.T.; Di Carlo, D. Hydrodynamic stretching of single cells for large population mechanical phenotyping. *Proc. Natl. Acad. Sci. USA* **2012**, *109*, 7630–7635. [[CrossRef](#)] [[PubMed](#)]
21. Yaginuma, T.; Oliveira, M.S.; Lima, R.; Ishikawa, T.; Yamaguchi, T. Human red blood cell behavior under homogeneous extensional flow in a hyperbolic-shaped microchannel. *Biomicrofluidics* **2013**, *7*, 054110. [[CrossRef](#)] [[PubMed](#)]
22. Otto, O.; Rosendahl, P.; Mietke, A.; Golfier, S.; Herold, C.; Klaue, D.; Girardo, S.; Pagliara, S.; Ekpenyong, A.; Jacobi, A.; *et al.* Real-time deformability cytometry: On-the-fly cell mechanical phenotyping. *Nat. Meth.* **2015**, *12*, 199–202. [[CrossRef](#)] [[PubMed](#)]
23. Shelby, J.P.; White, J.; Ganesan, K.; Rathod, P.K.; Chiu, D.T. A microfluidic model for single-cell capillary obstruction by Plasmodium falciparum infected erythrocytes. *Proc. Natl. Acad. Sci. USA* **2003**, *100*, 14618–14622. [[CrossRef](#)] [[PubMed](#)]
24. Rosenbluth, M.J.; Lam, W.A.; Fletcher, D.A. Analyzing cell mechanics in hematologic diseases with microfluidic biophysical flow cytometry. *Lab Chip* **2008**, *8*, 1062–1070. [[CrossRef](#)] [[PubMed](#)]
25. Hou, H.W.; Li, Q.S.; Lee, G.Y.H.; Kumar, A.P.; Ong, C.N.; Lim, C.T. Deformability study of breast cancer cells using microfluidics. *Biomed. Microdevices* **2009**, *11*, 557–564. [[CrossRef](#)] [[PubMed](#)]
26. Abkarian, M.; Faivre, M.; Stone, H.A. High-speed microfluidic differential manometer for cellular-scale hydrodynamics. *Proc. Natl. Acad. Sci. USA* **2006**, *103*, 538–542. [[CrossRef](#)] [[PubMed](#)]
27. Handayani, S.; Chiu, D.T.; Tjitra, E.; Kuo, J.S.; Lampah, D.; Kenangalem, E.; Renia, L.; Snounou, G.; Price, R.N.; Anstey, N.M.; *et al.* High deformability of Plasmodium vivax-infected red blood cells under microfluidic conditions. *J. Infect. Dis.* **2009**, *199*, 445–450. [[CrossRef](#)] [[PubMed](#)]
28. Quinn, D.J.; Pivkin, I.; Wong, S.Y.; Chiam, K.H.; Dao, M.; Karniadakis, G.E.; Suresh, S. Combined simulation and experimental study of large deformation of red blood cells in microfluidic systems. *Ann. Biomed. Eng.* **2011**, *39*, 1041–1050. [[CrossRef](#)] [[PubMed](#)]
29. Diez-Silva, M.; Park, Y.; Huang, S.; Bow, H.; Mercereau-Puijalon, O.; Deplaine, G.; Lavazec, C.; Perrot, S.; Bonnefoy, S.; Feld, M.S.; *et al.* Pf155/RESA protein influences the dynamic microcirculatory behavior of ring-stage Plasmodium falciparum infected red blood cells. *Sci. Rep.* **2012**, *2*, 614. [[CrossRef](#)] [[PubMed](#)]
30. Guo, Q.; Reiling, S.J.; Rohrbach, P.; Ma, H. Microfluidic biomechanical assay for red blood cells parasitized by Plasmodium falciparum. *Lab Chip* **2012**, *12*, 1143–1150. [[CrossRef](#)] [[PubMed](#)]
31. Huang, S.; Undisz, A.; Diez-Silva, M.; Bow, H.; Dao, M.; Han, J. Dynamic deformability of Plasmodium falciparum-infected erythrocytes exposed to artesunate *in vitro*. *Integr. Biol.* **2013**, *5*, 414–422. [[CrossRef](#)] [[PubMed](#)]
32. Kwan, J.M.; Guo, Q.; Kyluik-Price, D.L.; Ma, H.; Scott, M.D. Microfluidic analysis of cellular deformability of normal and oxidatively damaged red blood cells. *Am. J. Hematol.* **2013**, *88*, 682–689. [[CrossRef](#)] [[PubMed](#)]
33. Wu, T.; Feng, J.J. Simulation of malaria-infected red blood cells in microfluidic channels: Passage and blockage. *Biomicrofluidics* **2013**, *7*, 44115. [[CrossRef](#)] [[PubMed](#)]
34. Sakuma, S.; Kuroda, K.; Tsai, C.D.; Fukui, W.; Arai, F.; Kaneko, M. Red blood cell fatigue evaluation based on the close-encountering point between extensibility and recoverability. *Lab Chip* **2014**, *14*, 1135–1141. [[CrossRef](#)] [[PubMed](#)]

35. Guo, Q.; Duffy, S.P.; Matthews, K.; Santoso, A.T.; Scott, M.D.; Ma, H. Microfluidic analysis of red blood cell deformability. *J. Biomech.* **2014**, *47*, 1767–1776. [[CrossRef](#)] [[PubMed](#)]
36. Myrand-Lapierre, M.-E.; Deng, X.; Ang, R.R.; Matthews, K.; Santoso, A.T.; Ma, H. Multiplexed fluidic plunger mechanism for the measurement of red blood cell deformability. *Lab Chip* **2015**, *15*, 159–167. [[CrossRef](#)] [[PubMed](#)]
37. Herricks, T.; Antia, M.; Rathod, P.K. Deformability limits of Plasmodium falciparum-infected red blood cells. *Cell. Microbiol.* **2009**, *11*, 1340–1353. [[CrossRef](#)] [[PubMed](#)]
38. Bow, H.; Pivkin, I.V.; Diez-Silva, M.; Goldfless, S.J.; Dao, M.; Niles, J.C.; Suresh, S.; Han, J. A microfabricated deformability-based flow cytometer with application to malaria. *Lab Chip* **2011**, *11*, 1065–1073. [[CrossRef](#)] [[PubMed](#)]
39. Wood, D.K.; Soriano, A.; Mahadevan, L.; Higgins, J.M.; Bhatia, S.N. A biophysical indicator of vaso-occlusive risk in sickle cell disease. *Sci. Transl. Med.* **2012**, *4*, 123ra26. [[CrossRef](#)] [[PubMed](#)]
40. Zeng, N.F.; Ristenpart, W.D. Mechanical response of red blood cells entering a constriction. *Biomicrofluidics* **2014**, *8*, 064123. [[CrossRef](#)] [[PubMed](#)]
41. Gabriele, S.; Benoliel, A.M.; Bongrand, P.; Theodoly, O. Microfluidic investigation reveals distinct roles for actin cytoskeleton and myosin II activity in capillary leukocyte trafficking. *Biophys. J.* **2009**, *96*, 4308–4318. [[CrossRef](#)] [[PubMed](#)]
42. Sharei, A.; Zoldan, J.; Adamo, A.; Sim, W.Y.; Cho, N.; Jackson, E.; Mao, S.; Schneider, S.; Han, M.-J.; Lytton-Jean, A.; *et al.* A vector-free microfluidic platform for intracellular delivery. *Proc. Natl. Acad. Sci. USA* **2013**, *110*, 2082–2087. [[CrossRef](#)] [[PubMed](#)]
43. Khan, Z.S.; Vanapalli, S.A. Probing the mechanical properties of brain cancer cells using a microfluidic cell squeezer device. *Biomicrofluidics* **2013**, *7*, 11806. [[CrossRef](#)] [[PubMed](#)]
44. Mak, M.; Erickson, D. A serial micropipette microfluidic device with applications to cancer cell repeated deformation studies. *Integr. Biol.* **2013**, *5*, 1374–1384. [[CrossRef](#)] [[PubMed](#)]
45. Lee, L.M.; Liu, A.P. A microfluidic pipette array for mechanophenotyping of cancer cells and mechanical gating of mechanosensitive channels. *Lab Chip* **2015**, *15*, 264–273. [[CrossRef](#)] [[PubMed](#)]
46. Guo, Q.; Park, S.; Ma, H. Microfluidic micropipette aspiration for measuring the deformability of single cells. *Lab Chip* **2012**, *12*, 2687–2695. [[CrossRef](#)] [[PubMed](#)]
47. Luo, Y.N.; Chen, D.Y.; Zhao, Y.; Wei, C.; Zhao, X.T.; Yue, W.T.; Long, R.; Wang, J.B.; Chen, J. A constriction channel based microfluidic system enabling continuous characterization of cellular instantaneous Young's modulus. *Sens. Actuat. B Chem.* **2014**, *202*, 1183–1189. [[CrossRef](#)]
48. Lange, J.R.; Steinwachs, J.; Kolb, T.; Lautscham, L.A.; Harder, I.; Whyte, G.; Fabry, B. Microconstriction arrays for high-throughput quantitative measurements of cell mechanical properties. *Biophys. J.* **2015**, *109*, 26–34. [[CrossRef](#)] [[PubMed](#)]
49. Pereira, P.; Grandne, V.; Forel, J.M.; Gabriele, S.; Camara, M.; Theodoly, O. Passive circulating cell sorting by deformability using a microfluidic gradual filter. *Lab Chip* **2013**, *13*, 161–170. [[CrossRef](#)] [[PubMed](#)]
50. Mak, M.; Reinhart-King, C.A.; Erickson, D. Elucidating mechanical transition effects of invading cancer cells with a subnucleus-scaled microfluidic serial dimensional modulation device. *Lab Chip* **2013**, *13*, 340–348. [[CrossRef](#)] [[PubMed](#)]
51. Pereira, P.; Valignat, M.-P.; Bico, J.; Theodoly, O. Single cell rheometry with a microfluidic constriction: Quantitative control of friction and fluid leaks between cell and channel walls. *Biomicrofluidics* **2013**, *7*, 024111. [[CrossRef](#)] [[PubMed](#)]
52. Tsai, C.H.; Sakuma, S.; Arai, F.; Kaneko, M. A new dimensionless index for evaluating cell stiffness-based deformability in microchannel. *IEEE Trans. Bio Med. Eng.* **2014**, *61*, 1187–1195. [[CrossRef](#)] [[PubMed](#)]
53. Zhao, Y.; Zhao, X.T.; Chen, D.Y.; Luo, Y.N.; Jiang, M.; Wei, C.; Long, R.; Yue, W.T.; Wang, J.B.; Chen, J. Tumor cell characterization and classification based on cellular specific membrane capacitance and cytoplasm conductivity. *Biosens. Bioelectron.* **2014**, *57*, 245–253. [[CrossRef](#)] [[PubMed](#)]
54. Zhao, Y.; Chen, D.; Luo, Y.; Li, H.; Deng, B.; Huang, S.-B.; Chiu, T.-K.; Wu, M.-H.; Long, R.; Hu, H.; *et al.* A microfluidic system for cell type classification based on cellular size-independent electrical properties. *Lab Chip* **2013**, *13*, 2272–2277. [[CrossRef](#)] [[PubMed](#)]
55. Zhao, Y.; Chen, D.; Li, H.; Luo, Y.; Deng, B.; Huang, S.B.; Chiu, T.K.; Wu, M.H.; Long, R.; Hu, H.; *et al.* A microfluidic system enabling continuous characterization of specific membrane capacitance and cytoplasm conductivity of single cells in suspension. *Biosens. Bioelectron.* **2013**, *43*, 304–307. [[CrossRef](#)] [[PubMed](#)]

56. Chen, J.; Xue, C.; Zhao, Y.; Chen, D.; Wu, M.H.; Wang, J. Microfluidic Impedance Flow Cytometry Enabling High-Throughput Single-Cell Electrical Property Characterization. *Int. J. Mol. Sci.* **2015**, *16*, 9804–9830. [[CrossRef](#)] [[PubMed](#)]
57. Wan, J.; Ristenpart, W.D.; Stone, H.A. Dynamics of shear-induced ATP release from red blood cells. *Proc. Natl. Acad. Sci. USA* **2008**, *105*, 16432–16437. [[CrossRef](#)] [[PubMed](#)]
58. Szeto, G.L.; Van Egeren, D.; Worku, H.; Sharei, A.; Alejandro, B.; Park, C.; Frew, K.; Brefo, M.; Mao, S.; Heimann, M.; *et al.* Microfluidic squeezing for intracellular antigen loading in polyclonal B-cells as cellular vaccines. *Sci. Rep.* **2015**, *5*, 10276. [[CrossRef](#)] [[PubMed](#)]
59. Huang, S.B.; Zhao, Z.; Chen, D.Y.; Lee, H.C.; Luo, Y.N.; Chiu, T.K.; Wang, J.B.; Chen, J.; Wu, M.H. A clogging-free microfluidic platform with an incorporated pneumatically-driven membrane-based active valve enabling specific membrane capacitance and cytoplasm conductivity characterization of single cells. *Sens. Actuat. B Chem.* **2014**, *190*, 928–936. [[CrossRef](#)]
60. Beattie, W.; Qin, X.; Wang, L.; Ma, H. Clog-free cell filtration using resettable cell traps. *Lab Chip* **2014**, *14*, 2657–2665. [[CrossRef](#)] [[PubMed](#)]
61. Zhao, Y.; Chen, D.; Luo, Y.; Chen, F.; Zhao, X.; Jiang, M.; Yue, W.; Long, R.; Wang, J.; Chen, J. Simultaneous characterization of instantaneous Young's modulus and specific membrane capacitance of single cells using a microfluidic system. *Sensors* **2015**, *15*, 2763–2773. [[CrossRef](#)] [[PubMed](#)]
62. Chen, J.; Zheng, Y.; Tan, Q.; Shojaei-Baghini, E.; Zhang, Y.L.; Li, J.; Prasad, P.; You, L.; Wu, X.Y.; Sun, Y. Classification of cell types using a microfluidic device for mechanical and electrical measurement on single cells. *Lab Chip* **2011**, *11*, 3174–3181. [[CrossRef](#)] [[PubMed](#)]
63. Zheng, Y.; Shojaei-Baghini, E.; Azad, A.; Wang, C.; Sun, Y. High-throughput biophysical measurement of human red blood cells. *Lab Chip* **2012**, *12*, 2560–2567. [[CrossRef](#)] [[PubMed](#)]



© 2015 by the authors; licensee MDPI, Basel, Switzerland. This article is an open access article distributed under the terms and conditions of the Creative Commons by Attribution (CC-BY) license (<http://creativecommons.org/licenses/by/4.0/>).